JMEPEG (2023) 32:4315–4324
https://doi.org/10.1007/s11665-022-07397-w

TECHNICAL ARTICLE

Effect of Pre-quenching Temperature on Microstructure and Mechanical Properties of a Low-Alloyed TRIP-Aided Steel

J.N. Huang, Z.Y. Tang, H. Ding, and P.Q. Dai

Submitted: 10 April 2022 / Revised: 15 June 2022 / Accepted: 22 August 2022 / Published online: 28 September 2022

Different pre-quenching + two-stage heat treatments were conducted on a low-alloyed transformation-induced plasticity (TRIP)-aided steel. The results showed that combining pre-quenching with conventional two-stage heat treatment can refine the ferrite grains effectively and improve the mechanical properties of the experimental TRIP-aided steel. Simultaneously, it is beneficial to obtain granular, small blocky, lath-like, and film-like retained austenite (RA). With the pre-quenching temperature increasing from 0 to 900 °C, the average grain size of ferrite and RA decreased from 2.4 to 1.3 μm and 0.43 to 0.36 μm, respectively. Combined pre-quenching at 875 °C for 2 min with two-stage heat treatment, the investigated steel exhibited an outstanding combination of ultimate tensile strength (UTS) of 842 MPa, total elongation (TEL) of 32.5%, and UTS × TEL of 27.4 GPa % because of the grain refinement and sustained TRIP effect.

Keywords mechanical properties, microstructure, pre-quenching temperature, TRIP-aided steel

1. Introduction

As a typical advanced high strength steels, transformation-induced plasticity (TRIP) steels, consisting of ferrite, bainite, and retained austenite (RA), are forerunner in the automotive parts (Ref 1-5). However, with the development of automotive industry, the comprehensive mechanical properties of TRIP steel cannot meet the requirements of the automotive applications. Therefore, it is urgent to develop a new method to improve the mechanical properties of TRIP steel.

It seems most existing studies focus on optimizing the intercritical annealing (IA) temperature–time or isothermal bainite transformation temperature–time to maximize the mechanical properties of TRIP steel (Ref 6-12). However, these methods have a limited effect on enhancing the mechanical properties of TRIP steel. Consequently, several approaches were proposed to improve the mechanical properties of TRIP steel, such as adding some microalloying elements (Nb (Ref 13, 14), Mo (Ref 15), V (Ref 16], Ti (Ref 17), and Cu (Ref 18)) or adopting equal channel angular pressing (ECAP) process (Ref 19). While some of these methods increase the cost due to the addition of microalloying elements, some of them are not suitable for industrial production due to limited by the equipment and process requirements.

Different from the above ways, Zhang et al. (Ref 20) reported that adopting pre-quenching process prior to quenching and partitioning (Q&P) treatment in a low-alloyed steel can increase the RA stability. It is generally known that the RA stability is also important to the mechanical properties of TRIP steel (Ref 21-23). Considering the similarity between Q&P steel and TRIP steel, we proposed that the pre-quenching process can be introduced prior to the traditional two-stage heat treatment to improve the RA stability of TRIP steel.

Given that the influences of pre-quenching process on microstructure evolution and mechanical properties of TRIP steel are still unclear, four different heat treatments were designed in the present study to understand the effects of pre-quenching temperature on microstructure evolution and mechanical properties of TRIP steel.

2. Experimental

The chemical composition of experimental steel is listed in Table 1. The experimental ingot was melted in a 50-Kg vacuum furnace. The ingot was homogenized at 1200 °C for 2 h and then forged to rectangular slabs. The slabs were reheated to 1200 °C for 2 h and hot rolled to sheets with thickness of 3 mm. The hot rolling sheets were subsequently cold-rolled to 1mm in thickness.

To understand the effects of pre-quenching temperature on microstructure evolution and mechanical properties of TRIP steel, four different heat treatments were designed in this study (Fig. 1). The phase transformation temperatures (Ac_1, Ac_3, and Ms) of the investigated steel were first determined by

J.N. Huang and **P.Q. Dai**, School of Materials Science and Engineering, Fujian University of Technology, Fuzhou, China; and Fujian Provincial Key Laboratory of Advanced Materials Processing and Application, Fuzhou, China; and **Z.Y. Tang** and **H. Ding**, School of Materials Science and Engineering, Northeastern University, Shenyang, China; and Key Laboratory of Lightweight Structural Materials, Shenyang, Liaoning Province, China. Contact e-mails: huangjnd@163.com and tangzy@smm.neu.edu.cn.

dilatometer experiments. (Detailed preparations were described in our previous work (Ref 24).

The experimental sample was first austenitized at 825 °C for 3 min and then austempered at 410 °C for 3 min. Finally, this sample was cooling in air to ambient temperature, and hereafter, it is abbreviated as TRIP sample. Simultaneously, four different pre-quenching + two-stage heat treatments were applied to the experimental samples. First, the samples were subjected to pre-quenching in a salt bath at 825, 850, 875, and 900 °C for 2 min, respectively, and then quenched to the ambient temperature. For simplicity, they are abbreviated as 825Q sample, 850Q sample, 875Q sample, and 900Q sample, respectively. Subsequently, these samples were heat-treated in the same way as the TRIP sample. And, they are named as 825Q-TRIP sample, 850Q-TRIP sample, 875Q-TRIP sample, and 900Q-TRIP sample, respectively.

Flat dog bone-shaped tensile specimens made of heat-treated sheets along the rolling direction were machined with a width of 6 mm and a gauge length of 25 mm. Uniaxial tensile testing at a strain rate of 1.3×10^{-3} s^{-1} was performed on the SANSCMT5000 machine. Microstructure was characterized by field-emission scanning electron microscope (SEM) and transmission electron microscope (TEM). Samples for SEM observations were first electrolytically polished and then etched with 4% nital. Eight representative SEM micrographs were chosen for each sample to measure the ferrite content (V_F) based on the pixel method by Image Pro Plus 6.0. First, the concave polygonal ferrite grains in SEM micrographs were picked out and dyed by PS. Then, the total area of concave polygonal ferrite grains (A_F) and SEM micrograph (A_T) was measured by Image Pro Plus 6.0, respectively (repeated 8 times). Finally, the V_F= (A_{F1}+ A_{F2}+ A_{F3}+ A_{F4}+ A_{F5}+ A_{F6}+ A_{F7}+ A_{F8})/(A_{T1}+ A_{T2}+ A_{T3}+ A_{T4}+ A_{T5}+ A_{T6}+ A_{T7}+ A_{T8}), where A_{Fi} and A_{Ti} are the total area of concave polygonal ferrite grains (A_F) and SEM micrograph (A_T) of the i SEM micrograph, respectively. The sizes of fifty randomly selected ferrite grains were manually measured by Image Pro Plus 6.0 software, and then, the average size of ferrite grains (D_F) was calculated. The operating voltage for electron backscatter diffraction (EBSD) was 20 Kv, and the step size was 50 nm, respectively. For TEM studies, the samples were first mechanically ground and then punched into 3-mm-diameter disks. The disks were finally electro-polished at − 20 °C by a twin-jet polisher (Struers, Tenuol-5) using a solution of 95% alcohol and 5% perchloric acid.

Table 1 Chemical composition (wt. %) of the experimental steel

C	Si	Mn	Nb	P	S	Fe
0.21	1.40	1.47	0.025	0.0067	0.0018	Bal

X-ray diffraction (XRD) was used to measure the volume fraction of RA (V_γ). The V_γ was calculated using the following equation (Ref 25):

$$V_\gamma = \frac{1.4I_\gamma}{I_\alpha + 1.4I_\gamma}$$

where I_α is the integrated intensities of α-phase and I_γ is the integrated intensities of RA.

The average carbon content of RA (C_γ in mass %) is calculated by equation (Ref 19):

$$\alpha_\gamma = 0.3578 + 0.0033C_\gamma \quad \text{(Eq 2)}$$

where α_γ is a lattice parameter of austenite (Ref 24).

3. Results

3.1 Microstructure

Figure 2 exhibits the SEM micrographs of samples after pre-quenching at different temperatures. As shown in Fig. 2(a), the cold-rolled sample (without pre-quenching treated) presented a mixed structure of ferrite and pearlite. After pre-quenching at different temperatures, the microstructure of the 825Q sample, 850Q sample, and 875Q sample consisted of polygonal ferrite and martensite (Fig. 2b-d). In addition, when the pre-quenching temperature increased from 825 to 875 °C, the content and average size of ferrite decreased from 41.4 to 15.1% and 1.7 to 1.2 μm, respectively. As the pre-quenching temperature

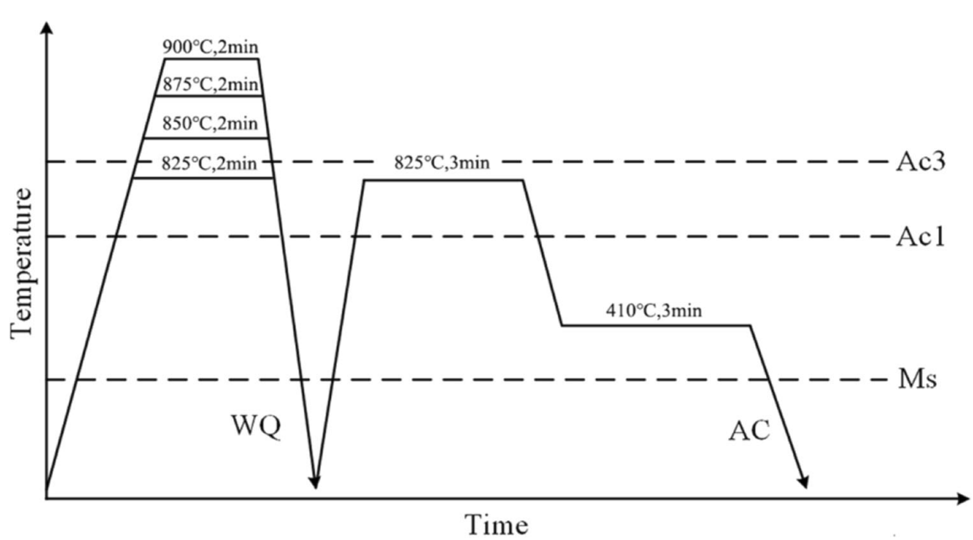

Fig. 1 Heat treatment schedules for producing experimental samples. (WQ: water quenched, AC: air cooling)

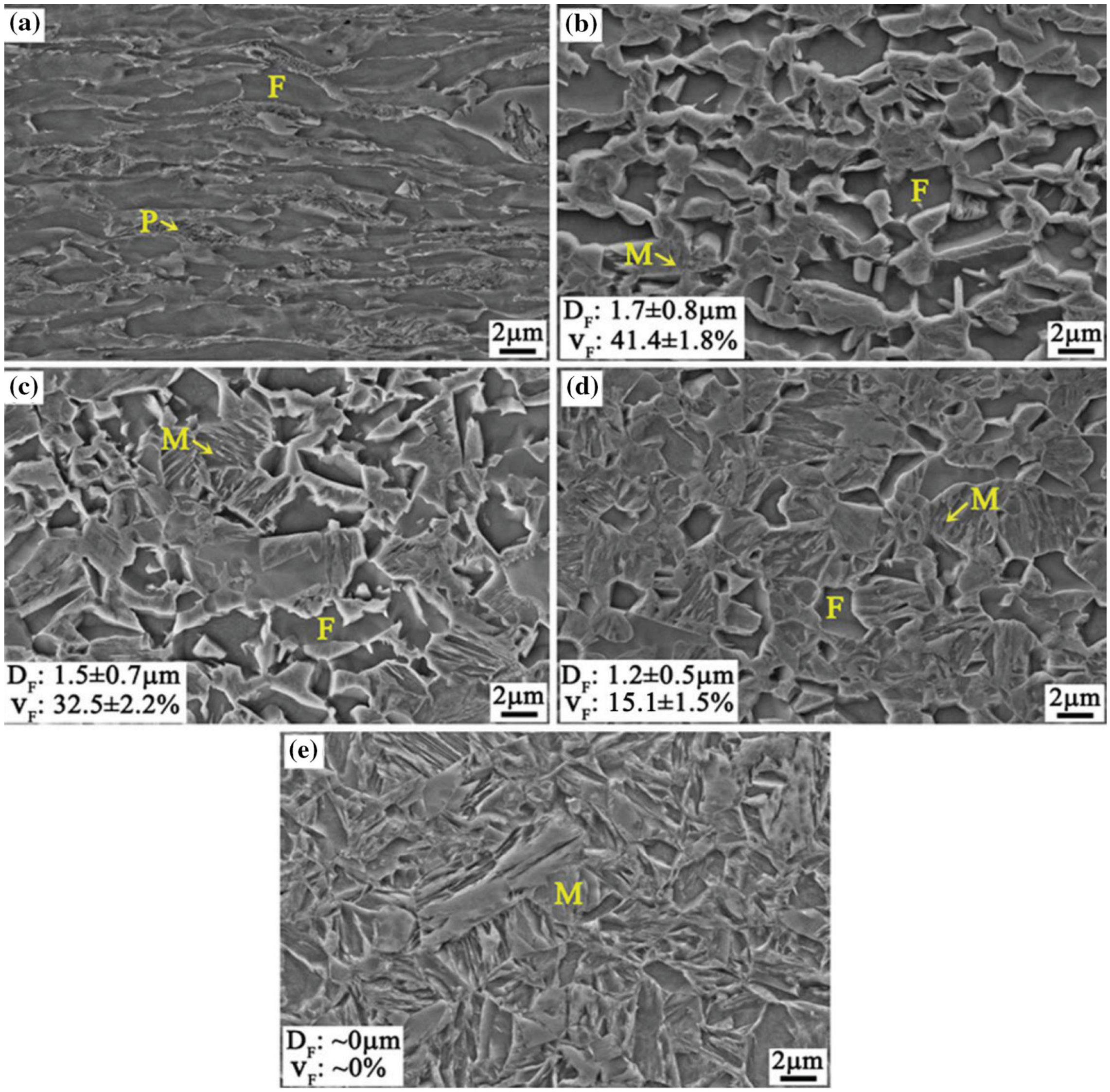

Fig. 2 SEM micrographs of (a) cold-rolled sample, (b) 825Q sample, (c) 850Q sample, (d) 875Q sample, (e) 900Q sample. (P: pearlite, F: ferrite, M: martensite)

reached 900 °C, the ferrite content decreased to 0% and the microstructure of 900Q sample was completely composed of martensite (Fig. 2e).

Figure 3 shows the SEM micrographs of samples suffered from different pre-quenching + two-stage heat treatments. Figure 3 shows that after different pre-quenching + two-stage heat treatments, the microstructure of all experimental samples was mainly composed of polygonal ferrite, granular bainite, and RA. The average size of ferrite grains of TRIP sample was 2.4 μm (Fig. 3a). Compared with Fig. 3(b-e) and Fig. 3(a), it is clear that after pre-quenching, the average size of ferrite grains of Q-TRIP samples was obviously smaller than that of the TRIP sample. More exactly, with pre-quenching temperature increasing to 825 °C and above, the average size of ferrite grains decreased from 1.9 μm to 1.3 μm (Fig. 3b-e).

EBSD technique was further conducted to detect the size of RA, and the typical results are indicated in Fig. 4. The α-bcc phases and RA are marked by blue and red, respectively. In the case without pre-quenching treatment, the average size of RA grains of TRIP sample was relatively large (0.43 μm) and majority of RA was located at the ferrite boundary, only a few distributed in ferrite grains (Fig. 4a). After pre-quenching treatment, the large blocky RA decreased accompanied by the increase in small blocky RA (Fig. 4c, e, g, i), which suggested that combining pre-quenching with two-stage heat treatment is beneficial to obtaining granular/small blocky RA. Simultaneously, with the pre-quenching temperature increasing from 825 to 900 °C, the average size of RA in 825Q-TRIP sample, 850Q-TRIP sample, 875Q-TRIP sample, and 900Q-TRIP sample changed slightly (∼ 0.36 μm); however, it was smaller than that of TRIP sample (0.43 μm) (Fig. 4b, d, f, h, j). This meant that the pre-quenching process can refine the RA grain size in a certain degree; however, it has a few effects on the RA grain size of Q-TRIP samples.

TEM was used to characterize the morphology of RA, and the results are shown in Fig. 5. For TRIP sample, blocky RA was presented in the ferrite grain (Fig. 5(a)). After different pre-quenching + two-stage heat treatments, granular RA and lath-like RA were appeared in 825Q-TRIP sample and 850Q-TRIP sample (Fig. 5(b, c)). In addition, when the pre-quenching

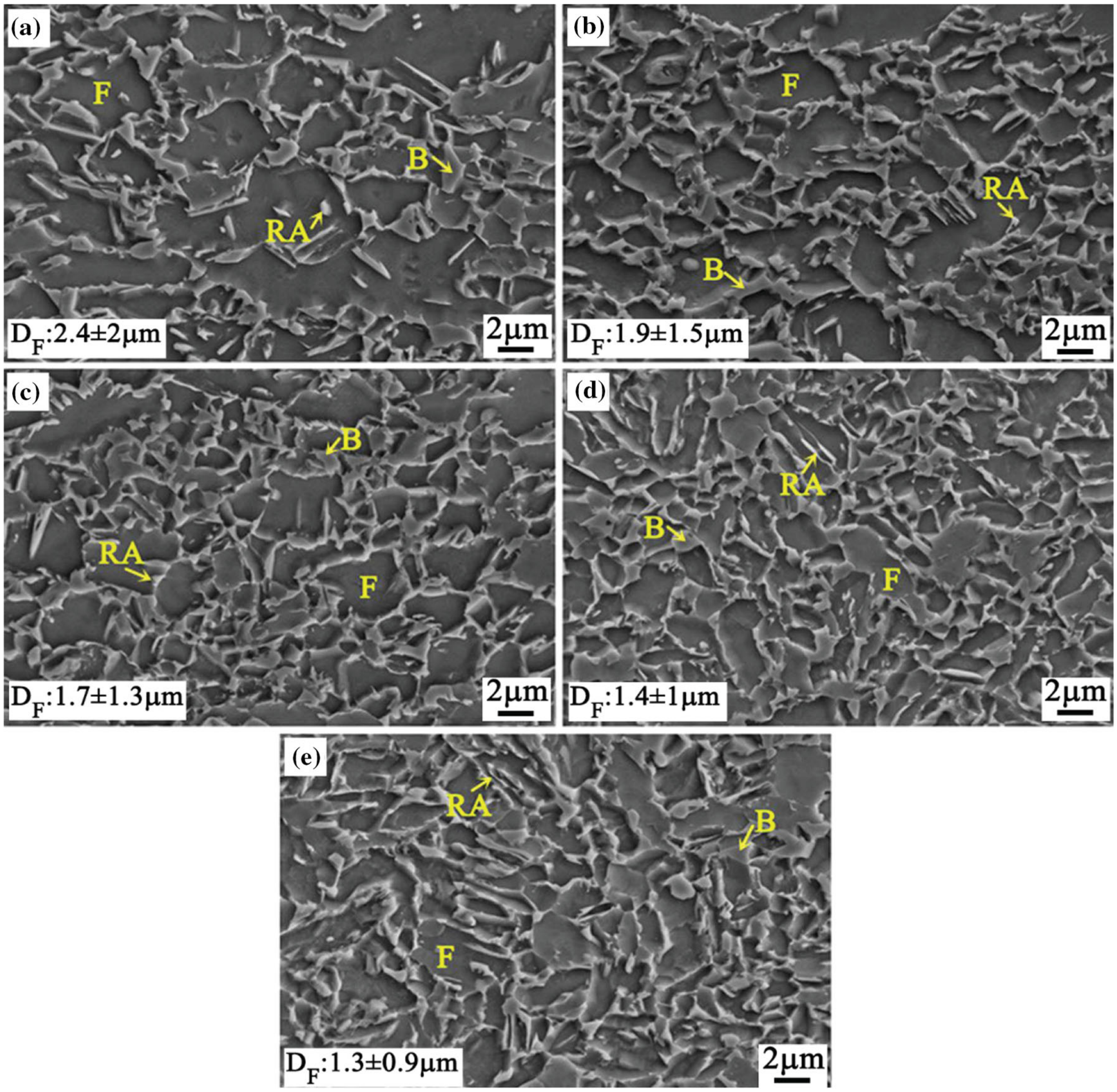

Fig. 3 SEM micrographs of (a) TRIP sample, (b) 825Q-TRIP sample, (c) 850Q-TRIP sample, (d) 875Q-TRIP sample, (e) 900Q-TRIP sample. (B: bainite, F:ferrite, RA: retained austenite)

temperature increased to 875 °C and 900 °C, the film-like RA increased in 875Q-TRIP sample and 900Q-TRIP sample (Fig. 5d, e). This phenomenon indicated that the pre-quenching + two-stage heat treatment is beneficial to obtaining lath-like RA and film-like RA.

The XRD patterns of experimental samples prior to and after tensile tests are presented in Fig. 6(a). It is clear that the peaks of γ-fcc phase (200_{γ}, $220_{\gamma,}$ and 311_{γ}) of all samples became weak after tensile deformation. Figure 6(b) shows the measured RA content of samples before and after tensile tests. The C concentration in RA of samples prior to tensile test is illustrated in Fig. 6(c). Based on the results of Fig. 6(b, c), the RA content and its C concentration of TRIP sample were 15.3 and 1.01 wt%, respectively. Both of them were relatively greater than that in Q-TRIP samples. With the pre-quenching temperature increasing from 825 to 900 °C, the RA content increased from 12.8 to 14.5%. Simultaneously, the C concentration in RA slightly decreased from 0.98 to 0.93 wt.%. After tensile deformation, the volume fraction of transformed RA of TRIP sample, 825Q-TRIP sample, 850Q-TRIP sample, 875Q-TRIP sample, and 900Q-TRIP sample was 10.1, 7.4, 7.9, 9.2, and 8.1%, respectively.

3.2 Mechanical Properties and Work Hardening Behavior

Figure 7(a) represents the engineering stress–strain curves of the samples after different heat treatments. The corresponding statistical results of the mechanical properties of these samples are given in Table 2. Combining Fig. 7(a) with Table 2, it can be found that TRIP sample exhibited the lowest yield strength (YS, 576 MPa), ultimate tensile strength (UTS, 833 MPa), total elongation (TEL, 28.4%), and the UTS × TEL (PSE, 23.7 GPa·%) compared with Q-TRIP samples. With the pre-quenching temperature increasing from 825 to 900 °C, the YS of the experimental sample increased monotonously from 623 to 692 MPa. The UTS was slightly changed from 840 MPa of 825Q-TRIP sample to 842 MPa of 875Q-TRIP sample. However, the UTS of 900Q-TRIP was 860 MPa. Both the TEL and PSE first increased from 30.4% and 25.5 GPa·% of 825Q-TRIP sample to 32.5% and 27.4 GPa·% of 875Q-TRIP sample, respectively. And then, when the pre-quenching temperature

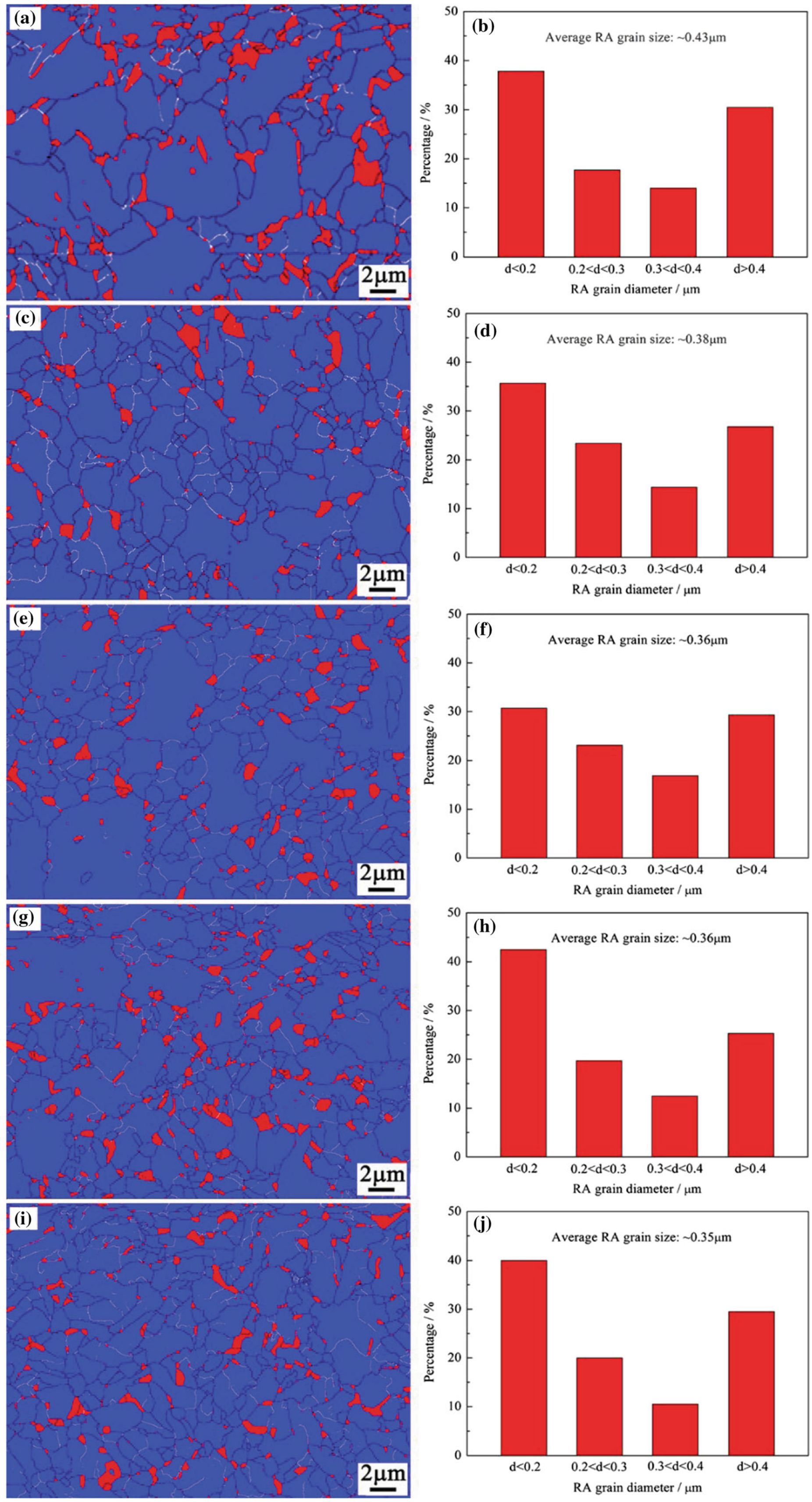

Fig. 4 EBSD maps of (a, b) TRIP sample, (c, d) 825Q-TRIP sample, (e, f) 850Q-TRIP sample, (g, h) 875Q-TRIP sample, (i, j) 900Q-TRIP sample

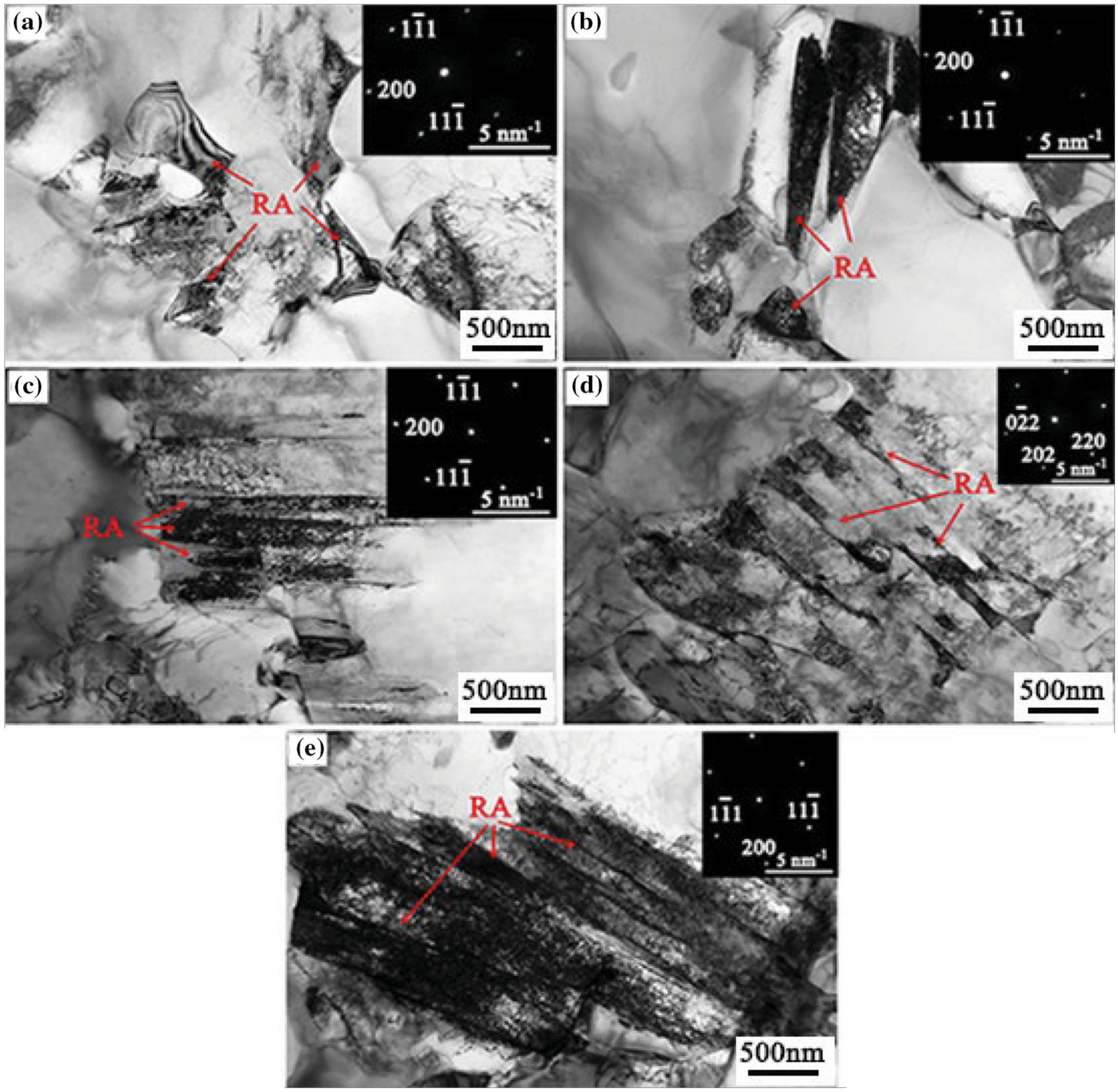

Fig. 5 TEM micrographs of (a) TRIP sample, (b) 825Q-TRIP sample, (c) 850Q-TRIP sample, (d) 875Q-TRIP sample, (e) 900Q-TRIP sample. (RA: retained austenite)

reached 900 °C, the TEL and PES of 900Q-TRIP sample were 30.5% and 26.2 GPa•%, showing a decreasing trend.

Figure 7(b) demonstrates the instantaneous strain hardening exponent (n) behavior with the true strain obtained from the tensile tests for experimental samples, where the n value was defined as $n = d \ln\sigma / d \ln\varepsilon$ (Ref 26). Figure 7(b) shows that the n value of all experimental samples can be divided into 2 stages. First, the n value increased sharply with the increase in true strain, which was due to the RA with lower stability transformed into martensite (Ref 27, 28) (stage 1). Subsequently, the n value increased slightly over a large strain range, because the sustained TRIP effect occurred (stage 2).

4. Discussion

4.1 Effect of Pre-quenching Temperature on Microstructure

As displayed in Fig. 3 and 4, it can be found that the pre-quenching temperature has a significant influence on the microstructure of TRIP steel. The detailed microstructure evolution from the cold-rolled microstructure (ferrite + pearlite) to the as-quenched microstructure (ferrite + martensite) after pre-quenching at different temperatures is illustrated in Fig. 2. The banded structure in cold-rolled sample disappeared after pre-quenching at different temperatures. With the pre-quenching temperature increasing from 825 to 900 °C, the volume fraction of austenite transformed from ferrite + pearlite constituents increased from 58.6 to 100% during annealing progress. And then, the austenite transformed into martensite as the sample was water quenched to ambient temperature, resulting in the decrease in volume fraction and average size of ferrite. For TRIP sample, the cold-rolled sample was first austenitized at 825 °C for 3 min. During this stage, the ferrite recovered and recrystallized and then grew up. Simultaneously, austenite nucleated at the C-rich region (such as the cementite particles in the pearlite colonies) and grew accompanying the carbides dissolve and C diffuses from ferrite to austenite (Ref 29, 30). Subsequently, the sample was fast quenched to 410 °C for 3 min. In this stage, the austenite

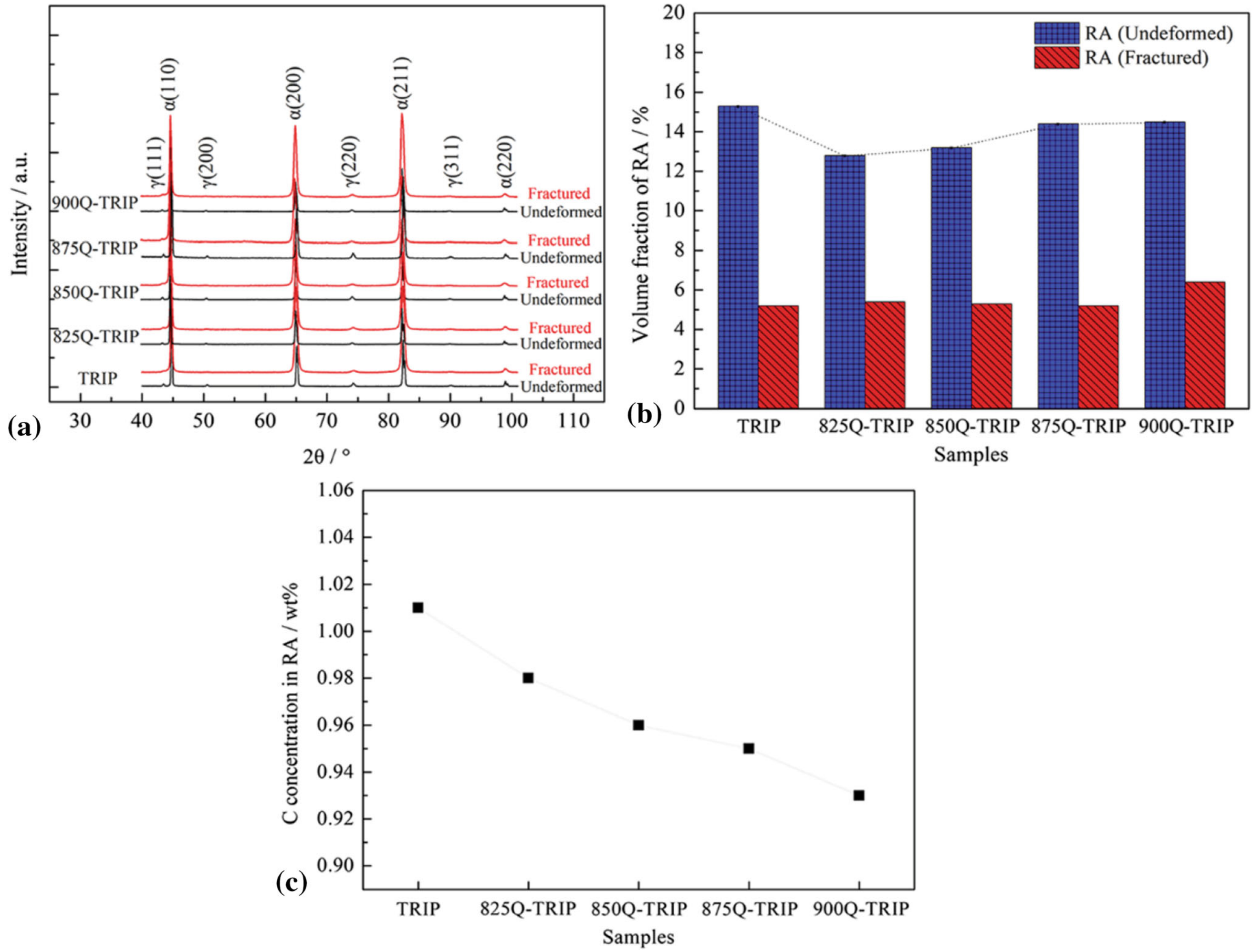

Fig. 6 (a) XRD patterns, (b) volume fraction of RA, (c) C concentration in RA

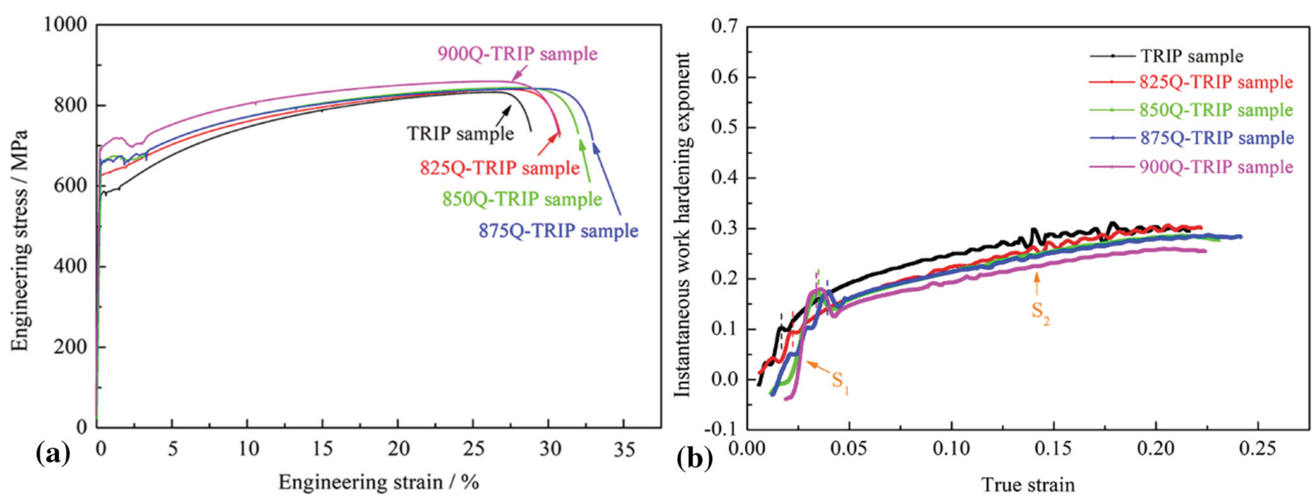

Fig. 7 (a) Engineering stress–strain curves of the experimental samples, (b) the instantaneous work hardening exponent (n) versus true strain. (S_1 and S_2 mean stages 1 and 2)

transformed into low C bainite with the excess C in bainite partitioned into adjacent RA, which further increased the C content in RA and stabilized the RA. For 825Q-TRIP sample, the same two-stage heat treatment as TRIP sample was applied on 825Q sample. As depicted in Fig. 2(b), the microstructure of 825Q sample consisted of martensite (58.6%) and ferrite (41.4%). The as-quenched lath martensite refined the prior austenite leading to the increase in the nucleation sites for

Table 2 Mechanical properties of the experimental samples after different heat treatments

Samples	YS, MPa	UTS, MPa	TEL, %	PSE, GPa·%
TRIP sample	576 (± 10)	833 (± 8)	28.4 (± 0.5)	23.7 (± 0.2)
825Q-TRIP sample	623 (± 8)	840 (± 5)	30.4 (± 0.4)	25.5 (± 0.2)
850Q-TRIP sample	657 (± 5)	842 (± 7)	31.3 (± 0.5)	26.4 (± 0.3)
875Q-TRIP sample	667 (± 9)	842 (± 10)	32.5 (± 0.7)	27.4 (± 0.3)
900Q-TRIP sample	692 (± 5)	860 (± 7)	30.5 (± 0.4)	26.2 (± 0.2)

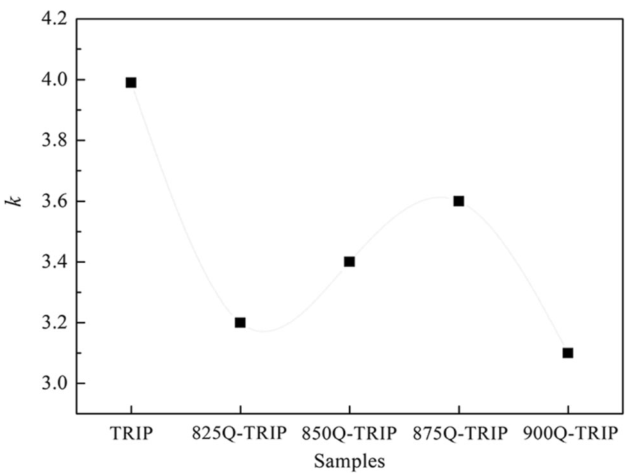

Fig. 8 Plots of k parameter of experimental samples after different pre-quenching + two-stage heat treatments

austenite and there had much smaller austenite formed during the subsequent IA process. Furthermore, these small austenite grains hindered the growth of recrystallized ferrite grains. Consequently, the finer microstructure appeared in 825Q-TRIP sample. Increasing the pre-quenching temperature from 825 to 900 °C resulted in an increase in the volume fraction of martensite from 58.6 to 100% and a decrease in the ferrite content from 41.4 to 0%. The increase in the volume fraction of lath martensite expanded the phase boundary, which further increased the nucleation sites for austenite. Thus, there had much smaller austenite grains formed during the IA process. Simultaneously, the recrystallized ferrite growth was further suppressed. As a result, the microstructure in Q-TRIP samples became finer and finer (Fig. 3b-e).

4.2 Effect of Pre-Quenching Temperature on Retained Austenite Stability

It is widely known that the RA stability plays a dominant role in governing the mechanical properties of TRIP steel (Ref 31, 32). As shown in Fig. 6(b), it can be deduced that the samples after different pre-quenching + two-stage heat treatments have different RA stabilities. In order to quantify the mechanical stability of RA in different samples, the equation (Ref 33]: $f_\gamma = f_{\gamma_0}\exp(-k\varepsilon)$ was used, where f_{γ_0} is the initial RA fraction, f_γ is the RA fraction at strain ε, and k is the mechanical stability of RA. A higher k value corresponds to lower austenite stability. It should be noted that the f_{γ_0}, f_γ, and ε of each sample were obtained from XRD results (Fig. 6) and tensile test results (Fig. 7), respectively. As shown in Fig. 8, the k value of TRIP sample was greater than that of Q-TRIP samples, which meant the RA stability in TRIP sample was relatively lower. This is because the TRIP sample had larger blocky RA and its average size of RA was largest (~ 0.43 μm) (Fig. 4). It is well known that the larger size of RA increases the martensite start (M_s) temperature, resulting in the decrease in RA stability (Ref 34, 35). With the pre-quenching temperature increasing from 825 to 900 °C, the k value was first increased from 3.2 of 825Q-TRIP sample to 3.6 of 875Q-TRIP sample, followed by a decrease to 3.1 of 900Q-TRIP sample. This implied that the stability of RA in Q-TRIP samples was first decreased and then increased. Figure 4 shows the pre-quenching annealing process had a few effects on the average size of RA of Q-TRIP samples (~ 0.36 μm), indicating that the RA size was not the critical factor on dictating the RA stability of Q-TRIP samples. As the pre-quenching temperature increased from 825 to 875 °C, the C concentration in RA decreased from 0.98 to 0.95% (Fig. 6), resulting in the slight decrease in RA stability. Because the C is a strong RA stabilizer, the stability of RA decreases with the decrease in C (Ref 36). According to Zhang et al. (Ref 20), the blocky RA has lower stability than the film-like RA. When the pre-quenching temperature reached 900 °C, the thickness of lath-like RA decreased (Fig. 5), which was the main reason why the RA stability of 900Q-TRIP sample was lowest.

4.3 Effect of Pre-quenching Temperature on Mechanical Properties

Combining Fig. 7(a) with Table 1, it can be found that with the pre-quenching temperature increasing from 0 (without pre-quenching process) to 900 °C, the YS of the experimental steel monotonically increased from 576 to 692 MPa. The YS (σ_y) can be estimated according to the Hall–Petch relationship (Ref 37): $\sigma_y = \sigma_0 + k_y d^{-1/2}$, where σ_0 k_y and d are the lattice friction stress, Hall–Petch coefficient, and mean grain size, respectively. As shown in Fig. 3, with the pre-quenching temperature increasing from 0 to 900 °C, the average size of ferrite grains decreased from 2.4 to 1.3 μm, which resulted in the increase in YS. As the pre-quenching temperature increased from 0 to 875 °C, the UTS did not show significant differences, which was ~ 840 MPa. However, the TEL of the experimental steel increased from 28.4 to 32.5%. For TRIP sample (the pre-quenching temperature was 0 °C), the highest amount of transformed RA (10.1%) resulted in largest Δσ (Δσ = UTS-YS = 257 MPa), which made up its lowest YS. Simultaneously, the RA in TRIP sample had lowest stability and majority of RA transformed into martensite, resulting in the highest n value during the early stage of tensile deformation (0 < ε < 0.17, Fig. 7b). Therefore, the TRIP effect cannot sustain at higher strain. This is also the main reason why the TRIP sample exhibited lowest TEL. Then, with the pre-quenching temperature increasing from 825 to 875 °C, the YS and the volume fraction of transformed RA increased accompanied by the decrease in volume fraction of rigid bainite. According to Wang et al. (Ref 29), the higher volume fraction of rigid bainite resulted in the higher tensile strength. Thus, the 825Q-TRIP sample, 850Q-TRIP sample, and 875Q-TRIP sample exhibited the similar UTS. Simultaneously, with the pre-quenching temperature increasing from 825 to 875 °C, the volume fraction of transformed RA increased from 7.4 to 9.2% (Fig. 6b) and the RA can sustainably transform into martensite at higher strain (Fig. 7b), meaning the better TRIP effect, which resulted in the TEL increased gradually. When the pre-quenching temperature reached 900 °C, the UTS of the 900Q-TRIP sample was increased to 860 MPa because of its highest YS, while the TEL decreased to 30.5% due to its weaker TRIP effect, and the amount of transformed RA decreased to 8.1% because the RA was too stable to transform into martensite at higher strain during tensile deformation.

5. Conclusions

In this study, the effects of pre-quenching temperature on microstructure evolution, RA stability, and mechanical properties of the Fe-1.47Mn-1.40Si-0.21C-0.025Nb TRIP-aided steel were investigated. The major conclusions are described as follows:

(1) Combining pre-quenching with two-stage heat treatment can refine the ferrite grains significantly. With the pre-quenching temperature increasing from 0 to 900 °C, the average size of ferrite grains decreased from 2.4 to 1.3 μm.
(2) Combining pre-quenching with two-stage heat treatment is beneficial to obtaining granular/small blocky RA. With the pre-quenching temperature increasing from 0 to 900 °C, the average size of RA grains decreased from 0.43 to 0.36 μm.
(3) Combining pre-quenching at 875 °C for 2 min with two-stage heat treatment, the investigated steel exhibited best combination of mechanical properties (UTS: 842 MPa, TEL: 32.5%, and UTS × TEL: 27.4 GPa•%).

Acknowledgments

The research was supported by the National Natural Science Foundation of China (Grant No. 51874088), Fundamental Research Funds for the Central Universities (Grant No. N2002015), Natural Science Foundation of Fujian Province (No. 2021J05224) and Scientific Research Foundation of Fujian University of Technology (GY-Z21009).

Data Availability

The raw/processed data required to reproduce these findings cannot be shared at this time as the data also form part of an ongoing study.

References

1. Z.L. Zeng, K.M. Reddy, S.X. Song, J.F. Wang, L. Wang, and X.D. Wang, Microstructure and Mechanical Properties of Nb and Ti Microalloyed Lightweight δ-TRIP Steel, *Mater. Charact.*, 2020, **164**, p 110324.
2. P. Xie, M. Han, C.L. Wu, Y.Q. Yin, K. Zhu, R.H. Shen, and J.H. Chen, A High-Performance TRIP Steel Enhanced by Ultrafine Grains and Hardening Precipitates, *Mater. Des.*, 2017, **127**, p 1–7.
3. M. Soleimani, A. Kalhor, and H. Mirzadeh, Transformation-Induced Plasticity (TRIP) in Advanced Steels: A Review, *Mater. Sci. Eng. A*, 2020, **795**, p 140023.
4. T.L. Wang, L.H. Qian, K.F. Li, F.C. Zhang, and J.Y. Meng, Strain-Hardening Behavior and Mechanisms of a Lamellar-Structured Low-Alloy TRIP Steel, *Mater. Sci. Eng. A*, 2021, **819**, p 141498.
5. B.C. De Cooman, Structure–properties Relationship in TRIP Steels Containing Carbide-free Bainite, *Curr. Opin. Solid State Mater. Sci.*, 2004, **8**(3–4), p 285–303.
6. A.K. Srivastava, G. Jha, N. Gope, and S.B. Singh, Effect of Heat Treatment on Microstructure and Mechanical Properties of Cold Rolled C-Mn–Si TRIP-aided Steel, *Mater. Charact.*, 2006, **57**(2), p 127–135.
7. Z.C. Zhang, K.I. Manabe, Y. Li, Y.M. Li, and F.X. Zhu, Effect of Isothermal Bainite Treatment on Microstructure and Mechanical Properties of Low-Carbon TRIP Seamless Steel Tube, *Steel Res. Int.*, 2012, **83**(7), p 645–652.
8. G. Adam, S. Adam, and R. Krzysztof, Mechanical Behavior and Stability of Dispersed Retained Austenite in Thermomechanically Rolled and Isothermally-Treated TRIP-Aided Multiphase Steel, *Mater. Sci. Eng. A*, 2022, **830**, p 142300.
9. Z.C. Zhang, Y.M. Li, X.W. Kong, K.I. Manabe, and N. Wang, Effect of Intercritical Annealing Time on Microstructure and Axial Mechanical Properties of TRIP Seamless Steel Tube, *Steel Res. Int.*, 2014, **85**(4), p 632–639.
10. H.X. Yin, Z.Z. Zhao, A.M. Zhao, X. Li, H.J. Hu, and J.T. Liang, Effect of Annealing Process on Microstructure and Mechanical Property of 1100 MPa Grade TRIP Steel, *J. Iron Steel Res. Int.*, 2015, **22**(7), p 622–629.
11. B. Zhang, L.X. Du, Y. Dong, D.X. Han, H.Y. Wu, F.H. Lu, and R.D.K. Misra, Structure-Property Relationship in Novel Low Carbon Hot-Rolled TRIP Steels via Thermo-Mechanical Controlled Processing and Coiling, *Mater. Sci. Eng. A*, 2020, **771**, p 138643.
12. X.L. Gu, Y.B. Xu, F. Peng, R.D.K. Misra, and Y. Wang, Role of Martensite/Austenite Constituents in Novel Ultra-High Strength TRIP-Assisted Steels Subjected to Non-Isothermal Annealing, *Mater. Sci. Eng. A*, 2019, **754**, p 318–329.
13. Y. Zou, Y. Han, H.S. Liu, H.X. Teng, M.S. Qiu, and F. Yang, Microstructure Evolution and Enhanced Mechanical Properties of a Novel Nb-Ti Micro-Alloyed Medium-Mn steel, *Mater. Charact.*, 2022, **187**, p 111828.
14. T. Bhattacharyya, S.B. Singh, S. Das, A. Haldar, and D. Bhattacharjee, Development and Characterisation of C-Mn–Al–Si–Nb TRIP Aided Steel, *Mater. Sci. Eng. A*, 2011, **528**, p 2394–2400.
15. B.J. Yoon and Y.S. Ahn, Effect of Mo Addition on Aging Behavior of TRIP-Aided Duplex Stainless Steel, *Mater. Charact.*, 2021, **173**, p 110946.
16. E. Abbasi and W.M. Rainforth, Microstructural Evolution of Nb–V–Mo and V Containing TRIP-assisted Steels during Thermomechanical Processing, *J. Mater. Sci. Technol.*, 2017, **33**, p 311–320.
17. A. Kammounia, W. Saikalya, M. Dumont, C. Marteau, X. Bano, and A. Charaï, Effect of the Bainitic Transformation Temperature on Retained Austenite Fraction and Stability in Ti Microalloyed TRIP Steels, *Mater. Sci. Eng. A*, 2009, **518**, p 89–96.
18. S.J. Kim, C.G. Lee, T.H. Lee, and C.S. Oh, Effect of Cu, Cr and Ni on Mechanical Properties of 0.15 wt.% C TRIP-Aided Cold Rolled Steels, *Scr. Mater.*, 2003, **48**, p 539–544.
19. Z.Y. Tang, J.N. Huang, H. Ding, Z.H. Cai, and R.D.K. Misra, Austenite Stability and Mechanical Properties of a Low-Alloyed ECAPed TRIP-Aided Steel, *Mater. Sci. Eng. A*, 2018, **724**, p 95–102.
20. J. Zhang, H. Ding, R.D.K. Misra, and C. Wang, Enhanced Stability of Retained Austenite and Consequent Work Hardening Rate Through Pre-quenching Prior to Quenching and Partitioning in a Q-P Microalloyed Steel, *Mater. Sci. Eng. A*, 2014, **611**, p 252–256.
21. H.N. El-Din and R. Reda, Retained Austenite Attributes and Mechanical Performance of Different Compositions of TRIP Steel Alloys, *J. Mater. Eng. Perf.*, 2019, **28**(4), p 2167–2177. https://doi.org/10.1007/s11665-019-04010-5
22. L. Liu, B.B. He, G.J. Cheng, H.W. Yen, and M.X. Huang, Optimum Properties of Quenching and Partitioning Steels Achieved by Balanc-

ing Fraction and Stability of Retained Austenite, *Scr. Mater.*, 2018, **150**, p 1–6.
23. T. Yamashita, S. Morooka, S. Harjo, T. Kawasaki, N. Koga, and O. Umezawa, Role of Retained Austenite in Low Alloy Steel at Low Temperature Monitored by Neutron diffraction, *Scr. Mater.*, 2020, **177**, p 6–10.
24. J.N. Huang, Z.Y. Tang, H. Ding, and R.D.K. Misra, The Significant Impact of Phase Fraction and Austenite Stability on the Mechanical Properties of a Low-Alloyed TRIP-Aided Steel: An Insight Into Experimental Analysis and Predictions, *Mater. Sci. Eng. A*, 2019, **759**, p 40–46.
25. N.H.V. Dijk, A.M. Butt, L. Zhao, J. Sietsma, S.E. Offerman, J.P. Wright, and S.V.D. Zwaag, Thermal Stability of Retained Austenite in TRIP Steels Studied by Synchrotron X-ray Diffraction during Cooling, *Acta Mater.*, 2005, **53**, p 5439–5447.
26. P.J. Jacques, J. Ladriere, and F. Delannay, On the Influence of Interactions between Phases on the Mechanical Stability of Retained Austenite in Transformation-Induced Plasticity Multiphase Steels, *Metall. Mater. Trans. A*, 2001, **32**, p 2759–2768.
27. Z.H. Cai, H. Ding, R.D.K. Misra, and Z.Y. Ying, Austenite Stability and Deformation Behavior in a Cold-Rolled Transformation-Induced Plasticity Steel with Medium Manganese Content, *Acta Mater.*, 2015, **84**, p 229–236.
28. J.N. Huang, Z.Y. Tang, H. Ding, H. Zhang, L.L. Bi, and R.D.K. Misra, Combining a Novel Cyclic Pre-quenching and Two-Stage Heat Treatment in a Low-Alloyed TRIP-Aided Steel to Significantly Enhance Mechanical Properties through Microstructural Refinement, *Mater. Sci. Eng. A*, 2019, **764**, p 138231.
29. C. Wang, H. Ding, M. Cai, and B. Rolfe, Characterization of Microstructures and Tensile Properties of TRIP-Aided Steels with Different Matrix Microstructure, *Mater. Sci. Eng. A*, 2014, **610**, p 65–75.
30. C. Wang, H. Ding, M. Cai, and B. Rolfe, Multi-phase Microstructure Design of a Novel High Strength TRIP Steel through Experimental Methodology, *Mater. Sci. Eng. A*, 2014, **610**, p 436–444.
31. S. Lee, S.J. Lee, and B.C. De Cooman, Austenite Stability of Ultrafine-Grained Transformation-Induced Plasticity Steel with Mn Partitioning, *Scr. Mater.*, 2011, **65**(3), p 225–228.
32. Z.H. Cai, H.Y. Li, S.Y. Jing, Z.C. Li, H. Ding, Z.Y. Tang, and R.D.K. Misra, Influence of Annealing Temperature on Microstructure and Tensile Property of Cold-Rolled Fe-0.2C-11Mn-6Al steel, *Mater. Charact.*, 2018, **137**, p 256–262.
33. J. Shi, X. Sun, M. Wang, W.J. Hui, H. Dong, and W.Q. Cao, Enhanced Work-Hardening Behavior and Mechanical Properties in Ultrafine-Grained Steels with Large-Fractioned Metastable Austenite, *Scr. Mater.*, 2010, **63**, p 815–818.
34. E. Jimenez-Melero, N.H.V. Dijk, L. Zhao, J. Sietsma, S.E. Offerman, J.P. Wright, and S.V.D. Zwaag, Characterization of Individual Retained Austenite Grains and Their Stability in Low-Alloyed TRIP Steels, *Acta Mater.*, 2007, **55**, p 6713–6723.
35. H.S. Yang and H.K.D.H. Bhadeshia, Austenite Grain Size and the Martensite-Start Temperature, *Scr. Mater.*, 2009, **60**, p 493–495.
36. Z.C. Li, R.D.K. Misra, H. Ding, H.P. Li, and Z.H. Cai, The Significant Impact of Pre-strain on the Structure-Mechanical Properties Relationship in Cold-Rolled Medium Manganese TRIP Steel, *Mater. Sci. Eng.*, 2018, **712**, p 206–213.
37. S. Takaki, Review on the Hall-Petch Relation in Ferritic Steel, *Mater. Sci. Forum*, 2010, **654–656**, p 11–16.